

Journal of Materials Chemistry C

Accepted Manuscript



This article can be cited before page numbers have been issued, to do this please use: D. Zhou, J. Li, L. Pang, D. Wang and I. M. Reaney, *J. Mater. Chem. C*, 2017, DOI: 10.1039/C7TC01718A.



This is an Accepted Manuscript, which has been through the Royal Society of Chemistry peer review process and has been accepted for publication.

Accepted Manuscripts are published online shortly after acceptance, before technical editing, formatting and proof reading. Using this free service, authors can make their results available to the community, in citable form, before we publish the edited article. We will replace this Accepted Manuscript with the edited and formatted Advance Article as soon as it is available.

You can find more information about Accepted Manuscripts in the [author guidelines](#).

Please note that technical editing may introduce minor changes to the text and/or graphics, which may alter content. The journal's standard [Terms & Conditions](#) and the ethical guidelines, outlined in our [author and reviewer resource centre](#), still apply. In no event shall the Royal Society of Chemistry be held responsible for any errors or omissions in this Accepted Manuscript or any consequences arising from the use of any information it contains.

Novel water insoluble and sustainable $(\text{Na}_x\text{Ag}_{2-x})\text{MoO}_4$ ($0 \leq x \leq 2$) microwave dielectric ceramics with spinel structure sintered at 410 degrees

Di Zhou,^{*a,b} Jing Li,^a Li-Xia Pang,^{b,c} Da-Wei Wang,^b and Ian M. Reaney^{*b}

^aElectronic Materials Research Laboratory, Key Laboratory of the Ministry of Education & International Center for Dielectric Research, Xi'an Jiaotong University, Xi'an 710049, Shaanxi, China

^bDepartment of Materials Science and Engineering, University of Sheffield, S1 3JD, UK

^cMicro-optoelectronic Systems Laboratories, Xi'an Technological University, Xi'an 710032, Shaanxi, China

Abstract

In the present work, a novel series of water insoluble ultra-low temperature firing $(\text{Na},\text{Ag})_2\text{MoO}_4$ microwave dielectric were prepared via the traditional solid state reaction method. A spinel structured solid solution was formed in the full composition range in the $(\text{Na}_x\text{Ag}_{2-x})\text{MoO}_4$ ($0 \leq x \leq 2$). As x increased from 0 to 2.0, cell volume decreased linearly from 9.32 Å to 9.10 Å. Sintering behavior were described using a so-called 'bowing' effect and densification was achieved below 420 °C for $0.5 \leq x \leq 1.2$ with grain size, 1 to 5 μm. Optimum microwave dielectric properties were obtained for $(\text{Na}_{1.2}\text{Ag}_{0.8})\text{MoO}_4$ ceramics sintered at 410 °C with a permittivity ~ 8.1, a microwave quality factor ~ 44,800 GHz and the temperature coefficient of the resonant frequency ~ - 82 ppm/°C at 13.9 GHz. Silver within the solid solution

^{*}Corresponding author E-mail address: zhoudi1220@gmail.com & d.zhou@sheffield.ac.uk (Di Zhou), i.m.reaney@sheffield.ac.uk (Ian M. Reaney)

inhibited hydrolyzation of ceramics and also reduced their sintering temperature.

[View Article Online](#)
DOI: 10.1039/C7TC01718A

Compared with the sintering temperatures of traditional microwave dielectric ceramic (Al_2O_3 , $> 1400\text{ }^\circ\text{C}$) and normal low temperature co-fired ceramics ($< 960\text{ }^\circ\text{C}$), this system will save lots of energy during processing and accelerate developments of sustainable electronic materials and devices.

I. Introduction

Microwave dielectric ceramics play an important role in modern communication devices with research dominated by the need for i), low loss (high quality value, Qf) materials with low permittivity ($\epsilon_r < 5$) ii), ceramics with large $\epsilon_r (> 150)$; iii), ultra high Qf materials ($> 100,000\text{ GHz}$) iv), lower cost materials fabricated from sustainable oxides resources and v), low sintering temperature ceramics, chemically compatible with low cost metal electrodes.¹⁻⁵

To meet the requirement of miniaturization, integration, and reliability, low temperature co-fired ceramic technology (LTCC) plays an important role in fabrication of modern microwave devices. LTCC technology is defined as the co-firing dielectric and internal electrode layers.^{3,6} LTCC technology requires microwave dielectric ceramics with lower sintering temperature than the melting point of metal electrode, such as $961\text{ }^\circ\text{C}$ for silver and $660\text{ }^\circ\text{C}$ for aluminum, along with chemical compatibility. Most traditional microwave dielectric ceramics have sintering temperature $> 961\text{ }^\circ\text{C}$ and thus require sintering aids, such as glasses and low melting point oxides to reduce processing temperatures but this is usually associated with deterioration of Qf .⁷⁻⁹

In recent years, so-called ultra-low temperature co-fired ceramic technology (ULTCC) has attracted much attention. In ULTCC, microwave dielectric ceramics can be densified without sintering aids since they are fabricated from intrinsically low

melting point oxides.¹⁰⁻¹⁴ A series of ULTCCs have been explored in Mo-rich, Bi-rich, Te-rich, B-rich, Li-rich, and V-rich systems, such as BaTe₄O₉ sintered at 550 °C with $\epsilon_r \sim 17.5$, Qf value $\sim 54,700$ GHz and temperature coefficient of frequency (TCF) ~ -90 ppm/°C,¹⁰ Bi₂Mo₂O₉ sintered at 620 °C with $\epsilon_r \sim 38$, Qf value $\sim 12,500$ GHz and TCF $\sim +31$ ppm/°C,¹¹ (Li,Bi)(Mo,V)O₄ with $\epsilon_r > 75$, Qf value $> 8,000$ GHz.¹² Such low sintering temperatures make it possible to employ Al in the multi-layer co-fired fabrication method. A prototype multilayer capacitor with five active layers sintered at 640 °C using Bi₂Mo₂O₉ as the dielectric and Al as an electrode layer was reported in our previous work.¹⁵ In the last decade, many MoO₃ based microwave dielectric ceramics have been explored due to their low melting point, $\sim 795^\circ\text{C}$. However, the MoO₃ is water soluble and molybdate-based microwave dielectric ceramics can suffer from surface degradation due to reaction with atmospheric moisture. Examples of water soluble molybdate ceramics include, Li₂O-MoO₃, Na₂O-MoO₃ and K₂O-MoO₃ etc.¹⁶⁻¹⁸ Li₂MoO₄ was first reported¹⁶ as a microwave dielectric ceramic with a $\epsilon_r \sim 5.5$, Qf value $\sim 46,000$ GHz, TCF ~ -160 ppm/°C, and a low sintering temperature $\sim 540^\circ\text{C}$. Subsequently, Kähari et al.^[19] reported that dense ceramics can be obtained by moistening Li₂MoO₄ powders at 120 °C and a pressure of 130 MPa due to re-crystallization during the volatilization of water, which can be represented as a pressure-mediated hydrothermal method. Li₂MoO₄ may also be used to fabricate dense composite ceramics, such as Li₂MoO₄-TiO₂, Li₂MoO₄-BaTiO₃ as well as organic-inorganic composites at $< 150^\circ\text{C}$.²⁰⁻²² It is evident that water soluble microwave dielectric materials may play an important role in the novel low temperature fabrication of electronic materials but for high Qf applications whose surfaces are exposed to ambient, water solubility is detrimental in achieving extended lifetimes. In previous work, Bi₂O₃, Ag₂O and ZnO effectively suppressed the

hygroscopicity of molybdates, such as $\text{Bi}_2\text{Mo}_2\text{O}_9$, Ag_2MoO_4 and $\text{Li}_2\text{Zn}_2\text{Mo}_3\text{O}_{12}$.^{5,11,23} New Article Online
DOI: 10.1039/C7TC01718A

Water insoluble microwave dielectric ceramics are essential for industry since they can be easily manufactured by using traditional solid state reaction method and with device geometries optimized through tape-casting and screen printing. In 2014, novel spinel structured water insoluble NaAgMoO_4 compound was reported with $\epsilon_r \sim 7.9$, $Qf \sim 33,000$ GHz and TCF ~ -120 ppm/ $^\circ\text{C}$ and sintered at 400 $^\circ\text{C}$ which is the lowest conventional sintering temperature yet reported for ULTCC.¹⁴

Generally, ULTCCs occur in low eutectic point oxides. NaAgMoO_4 is spinel structured with general formula A_2BO_4 , in which oxygen ions form a cubic close-packed array with 8 out of 64 tetrahedra (T_d) and 16 out of 32 octahedra (O_h) occupied within the structure.^{24,25} Spinel structure is ubiquitous, highly adaptive and a number of spinel structured materials have been widely studied due to their magnetic,²⁶ dielectric²⁷ and semi-conducting properties.²⁸ Besides NaAgMoO_4 , Ag_2MoO_4 and Na_2MoO_4 are also spinel structured^{23,29,30} In general, Ag-based oxides are insoluble with respect to Li, Na and K counterparts.^{31,32} Hence compositions in the solid solution $(\text{Na,Ag})_2\text{MoO}_4$ look attractive to avoid reaction with ambient moisture. Moreover, modifying the Na:Ag ratio may tune TCF closer to zero. Hence, this solid solution is considered ideal to potentially synthesize temperature-stable ULTCC compositions suitable for MW applications.

II. Experimental

Reagent-grade Na_2CO_3 , Ag_2CO_3 , and MoO_3 (>99%, Fuchen Chemical Reagents, Tianjin, China) were weighed according to the stoichiometric formulation $(\text{Na}_x\text{Ag}_{2-x})\text{MoO}_4$ ($x=0, 0.5, 1.0, 1.2, 1.5, 1.8, 2.0$). Powders were mixed and milled for 4 h using a planetary mill. The powder mixture was then dried and calcined at $350 \sim 550$ $^\circ\text{C}$ for 4 h. The calcined powders were ball milled for 4.5 h to obtain fine powders.

and pressed into cylinders (10 mm in diameter and 4 ~ 5 mm in height) at 100 MPa. View Article Online
DOI: 10.1039/C7TC01718A

Samples were sintered 2 h at 380 °C to 620 °C. Room temperature X-ray diffraction (XRD) was performed using with CuK α radiation (Rigaku D/MAX-2400 X-ray diffractometry, Tokyo, Japan) from 10-80 °2 θ at a step size of 0.02 °. The results were analyzed by the Rietveld profile refinement method, using FULLPROF program. As-fired and fractured surfaces were observed by using a scanning electron microscopy (SEM, FEI, Quanta 250 F). Dielectric properties at microwave frequency were measured with the TE_{01 δ} dielectric resonator method with a network analyzer (HP 8720 Network Analyzer, Hewlett-Packard) and a temperature chamber (Delta 9023, Delta Design, Poway, CA). The temperature coefficient of resonant frequency TCF (τ_f) was calculated with the following formula:

$$TCF(\tau_f) = \frac{f_T - f_{T_0}}{f_{T_0} \times (T - T_0)} \times 10^6 \quad (1)$$

where f_T and f_{T_0} are the TE_{01 δ} resonant frequencies at temperature T and T₀, respectively.

III. Results and discussions

X-ray diffraction patterns of the (Na_xAg_{2-x})MoO₄ (0 ≤ x ≤ 2) ceramics sintered at optimal temperatures are presented in Figure 1a. All compositions crystallized in the spinel structure with no second phase peaks apparent in the spectra, suggesting that the spinel structure is stable for the (Na_xAg_{2-x})MoO₄ (0 ≤ x ≤ 2). With increased Na concentration, the relative intensity of the (111) and (220) peaks increased accompanied by a decrease in (222) and (440). Refinements were performed on the (Na_{1.2}Ag_{0.8})MoO₄ and (Na_{1.8}Ag_{0.2})MoO₄ samples using Fullprof software based on the XRD data. As shown in Figure 1b and 1c, the refined cell parameters are $a = b = c = 9.202$ (0) Å and 9.133 (5) Å for the (Na_{1.2}Ag_{0.8})MoO₄ ($R_p = 11.9$ %, $R_{wp} = 14.3$ %,

and $R_{\text{exp}} = 7.07 \%$) and $(\text{Na}_{1.8}\text{Ag}_{0.2})\text{MoO}_4$ ($R_p = 8.32 \%$, $R_{\text{wp}} = 10.5 \%$, and $R_{\text{exp}} = 5.91 \%$), respectively, each arising from a face centered cubic structure with space group Fd-3m, based on the model (ICSD #159740) reported by Bouhemadou et al.³³ All cell parameters are listed in Table I and II and a schematic crystal structure of the $(\text{Na}_x\text{Ag}_{2-x})\text{MoO}_4$ ($0 \leq x \leq 2$) sample is presented in the insert of Figure 1e.³⁴ Na and Ag cations are randomly arranged in the CN6, octahedra, whereas the Mo cations are tetrahedrally (CN4) coordinated. Cell parameters of the $(\text{Na}_x\text{Ag}_{2-x})\text{MoO}_4$ ($0 \leq x \leq 2$) ceramics as a function of x value are shown in Figure 1f which decrease almost linearly with the increase of x in accordance with Vegard's law which may be explained by the larger ionic radius of Ag^+ (1.15 Å) with respect to Na^+ (1.02 Å) in CN6.³⁵ For the $(\text{Na}_{1.2}\text{Ag}_{0.8})\text{MoO}_4$ co-fired samples with both silver and aluminum, only peaks of the spinel phase and respective metals are observed with no additional peaks in the XRD traces, implying that $(\text{Na}_{1.2}\text{Ag}_{0.8})\text{MoO}_4$ material did not react with either Ag or Al at 410 °C.

SEM images of as-fired and fractured surfaces of the $(\text{Na}_{1.2}\text{Ag}_{0.8})\text{MoO}_4$ ceramic sintered 410 °C are shown in Figure 2a. A dense and homogeneous microstructure is observed in the $(\text{Na}_{1.2}\text{Ag}_{0.8})\text{MoO}_4$ ceramic sintered at 410 °C with grain size 1 ~ 5 μm, similar to $(\text{NaAg})\text{MoO}_4$ and smaller than that of pure Ag_2MoO_4 .^{14,23} The densification temperature and relative densities (theoretical density was obtained from cell parameters shown in Figure 1; bulk densities for $x < 1.5$ were obtained using Archimedes' method and for $x \geq 1.5$ sample simply using mass / volume) of the $(\text{Na}_x\text{Ag}_{2-x})\text{MoO}_4$ ($0 \leq x \leq 2$) ceramics as a function of x are shown in Figure 2b. Sintering temperatures of the two end members, Ag_2MoO_4 and Na_2MoO_4 , are 450 °C and 620 °C, respectively.^{17,23} The sintering temperature did not change linearly but went through a minimum of 400 °C at $x = 0.1$, behavior previously observed in solid

solutions such as $\text{Bi}(\text{Sb}_{1-x}\text{Ta}_x)\text{O}_4$ and $(\text{Ag,Bi})(\text{Mo,V})\text{O}_4$.^{36,37} This 'bow-shaped' behavior extends even to, for example, calculation of the band gap in ZnO–CrO,

III–V compounds,^{38, 39} and is described by the following second order equation:

$$S.T.(x) = 0.5xS.T.(\text{Na}_2\text{MoO}_4) + (1 - 0.5x) \times S.T.(\text{Ag}_2\text{MoO}_4) - bx(1 - 0.5x) \quad (2)$$

where $S.T.(\text{Na}_2\text{MoO}_4)$ and $S.T.(\text{Ag}_2\text{MoO}_4)$ correspond to sintering temperatures of the end member Na_2MoO_4 and Ag_2MoO_4 , respectively. The parameter b is the bowing parameter which is influenced by a number of different crystal chemical factors such as the difference in ionic radius and electronegativity. When fitted to Eq. (2), the observed nonlinearity in sintering temperatures of the $(\text{Na}_x\text{Ag}_{2-x})\text{MoO}_4$ ($0 \leq x \leq 2$) ceramics yielding a bowing parameter, $b = 248.6$ °C.

The spinel structure primitive cell contains two Ag_2MoO_4 units that provide a total of 42 vibrational degrees of freedom. Group theoretical considerations give rise to five Raman-active modes:⁴⁰⁻⁴³

$$\Gamma = A_{1g} + E_g + 3F_{2g} \quad (3)$$

As shown in Figure 3a, the A_{1g} mode at ~ 890 cm^{-1} corresponds to the Mo–O bond symmetric stretching vibration of the MoO_4 unit, whereas the T_{2g} mode at 780 cm^{-1} represents asymmetric stretching. The F_{2g} mode found at 370 cm^{-1} corresponds to the asymmetric bending mode of the MoO_4 units. The E_g mode at 279 cm^{-1} corresponds to a twofold degenerate E_g symmetric bending mode of the MoO_4 units. As reported in the literature, there should be another F_{2g} mode at about 100 cm^{-1} , which corresponds to triply degenerate F_{2g} associated with translations of the MoO_4 units (or Ag cations). Due to the measurement limit, this mode was not obtained here. Wavenumbers of the stretching and bending modes of the $(\text{Na}_x\text{Ag}_{2-x})\text{MoO}_4$ ($0 \leq x \leq 2$) ceramics as a function of x are presented in Figure 3b. All the modes were blue-shifted as a function of x . Hardcastle and Wachs⁴⁴ gave a empirical relation

between Raman stretching frequencies of molybdenum-oxygen bonds and their respective bond distances in molybdenum oxide compounds in 1990 as following:

$$\nu(\text{cm}^{-1}) = 32895 \times \exp(-2.073R) \quad (4)$$

where ν is the Raman shift and R is the Mo-O bond distance. The calculated Mo-O bond length lies between 1.741 ~ 1.749 Å as shown in Figure 3b. The Mo-O bond length decreased linearly with x in $(\text{Na}_x\text{Ag}_{2-x})\text{MoO}_4$, corresponding well with the XRD analysis discussed above.

Microwave dielectric ϵ_r , Qf and TCF of the $(\text{Na}_x\text{Ag}_{2-x})\text{MoO}_4$ ($0 \leq x \leq 2$) ceramics as a function of x are shown in Figure 4. Microwave dielectric properties as a function of sintering temperature were not shown for clarity and the densification temperatures were obtained from both density and permittivity as a function of sintering temperature. ϵ_r is stable at ~ 8 for $0 \leq x \leq 1.2$ but then decreases to ~ 5 for $1.5 \leq x \leq 2.0$. The ionic polarizability of Na^+ is reported by Shannon to be 1.80 Å³, whilst that of Ag^+ was calculated as 2.25 Å³ in previous work.^{14,45} Microwave ϵ_r is determined by photon absorption and far-infrared region of the EM spectrum and only ionic and electron displacive polarization contributes. Typically, microwave ϵ_r changes linearly in solid solution materials as described by Shannon's additive rule but the sudden drop between $1.2 \leq x \leq 1.5$ does not follow the predicted trend. The polarizability of Mo^{6+} is ~ 3.28 Å³,^{46,47} larger than those of Na^+ and Ag^+ . Therefore it is Mo^{6+} ion within the MoO_4 tetrahedron which contributes primarily to ϵ_r in the $(\text{Na}_x\text{Ag}_{2-x})\text{MoO}_4$ ($0 \leq x \leq 2$) system. As discussed previously, the smaller ionic radius of Na^+ with respect to Ag^+ decreases the dimensions of the $[\text{Na},\text{Ag}]\text{O}_6$ octahedra, resulting in a linear decrease in cell volume with MoO_4 tetrahedra forced to accommodate the decreasing cell volume. The effective polarizability of Mo^{6+} ion is thus reduced as the

Mo-O bond length shrinks. Although this simple concept explains the decrease in ϵ_r , it does not explain the non-linear trend and this phenomena requires further study.

Qf values of this system increased from below 20,000 GHz to above 40,000 GHz as x increased from 0 to above 1.2, concomitant with a shift in TCF from ~ -140 ppm/ $^{\circ}\text{C}$ at $x = 0$ to ~ -60 ppm/ $^{\circ}\text{C}$ at $x = 2.0$. The best microwave dielectric properties were obtained for the $(\text{Na}_{1.2}\text{Ag}_{0.8})\text{MoO}_4$ ceramic sintered 410°C with a $\epsilon_r \sim 8.1$, Qf value = 44,800 GHz and TCF = -82 ppm/ $^{\circ}\text{C}$ at 13.9 GHz. Comparison of its microwave dielectric properties with other systems with a permittivity ~ 8 from literatures are presented in Table 3.^{5,14,16,23,48} Moreover, the substitution of Ag up to 10 mol. % for Na ($x=1.8$), effectively suppresses hydrolyzation which, in combination with the chemical compatibility of these ceramics with Al and Ag electrodes, suggests that they have potential for exploitation in ULTCC technology.

IV. Conclusions

In summary, a spinel structured solid solution was formed in the $(\text{Na}_x\text{Ag}_{2-x})\text{MoO}_4$ ($0 \leq x \leq 2$) ceramics prepared via solid state reaction method. The cell volume and Mo-O bond length both decreased with x . Within the composition range $0.5 \leq x \leq 1.2$, ceramics densified below 420°C with microwave $\epsilon_r \sim 8$, $30,000 < Qf < 44,800$ GHz and values between $-120 \leq \text{TCF} \leq -82$ ppm/ $^{\circ}\text{C}$. Combined with our previous study illustrating the chemically compatible with silver and aluminum electrodes, these compositions have the potential to play an important role in ULTCC technology.

Acknowledgements

This work was supported by the National Natural Science Foundation of China (U1632146), the Young Star Project of Science and Technology of Shaanxi Province (2016KJXX-34), the Fundamental Research Funds for the Central University, and the 111 Project of China (B14040). The SEM work was done at International Center for

Dielectric Research (ICDR), Xi'an Jiaotong University, Xi'an, China and the authors

[View Article Online](#)
DOI: 10.1039/C7TC01718A

thank Ms. Yan-Zhu Dai for her help in using SEM. Ian M. Reaney would like to acknowledge the Sustainability and Substitution of Functional Materials and Devices EPSRC (EP/L017563/1) and Engineering and Physical Sciences Research Council grant, EP/N010493/1.

References

View Article Online
DOI: 10.1039/C7TC01718A

- 1 I. M. Reaney & D. Iddles, *J. Am. Ceram. Soc.*, 2006, **89**, 2063.
- 2 R. J. Cava, *J. Mater. Chem.*, 2001, **11**, 54.
- 3 M. T. Sebastian, H. Jantunen, *Int. Mater. Rev.*, 2008, **53**, 57.
- 4 H. T. Kim, S. H. Kim, S. Nahm, J. D. Byun and Y. Kim, *J. Am. Ceram. Soc.*, 1999, **82**, 3043.
- 5 D. Zhou, C. A. Randall, L. X. Pang, H. Wang, X. G. Wu, J. Guo, G. Q. Zhang, L. Shui and X. Yao, *J. Am. Ceram. Soc.*, 2011, **94**, 802.
- 6 L. X. Pang, D. Zhou, Z. M. Qi, W. G. Liu, Z. X. Yue and I. M. Reaney, *J. Mater. Chem. C*, 2017, **5**, 2695.
- 7 H. Jantunen, R. Rautioaho, A. Uusimäki and S. Leppavuori, *J. Eur. Ceram. Soc.*, 2010, **20**, 2331.
- 8 H. Kagata, T. Inoue, J. Kato and I. Kameyama, *Jpn. J. Appl. Phys.*, 1992, **31**, 3152.
- 9 L. X. Pang and D. Zhou, *J. Am. Ceram. Soc.*, 2010, **93**, 3614.
- 10 D. K. Kwon, M. T. Lanagan and T. R. Shrout, *J. Am. Ceram. Soc.*, 2005, **88**, 3419.
- 11 D. Zhou, H. Wang, X. Yao and L. X. Pang, *J. Am. Ceram. Soc.*, 2008, **91**, 3419.
- 12 D. Zhou, L. X. Pang, J. Guo, Z. M. Qi, T. Shao, X. Yao, C. A. Randall, *J. Mater. Chem.*, 2012, **22**, 21412.
- 13 L. X. Pang, D. Zhou, J. Guo, Z. X. Yue and X. Yao, *J. Am. Ceram. Soc.*, 2015, **98**, 130.
- 14 D. Zhou, L. X. Pang, Z. M. Qi, B. B. Jin, X. Yao, *Sci. Rep.*, 2014, **4**, 5980.
- 15 D. Zhou, C. A. Randall, A. Baker, H. Wang, L. X. Pang and X. Yao, *J. Am. Ceram. Soc.*, 2010, **93**, 1443.
- 16 D. Zhou, C. A. Randall, H. Wang, L. X. Pang and X. Yao, *J. Am. Ceram. Soc.*, 2010, **93**, 1096.

- 17 G. Q. Zhang, H. Wang, J. Guo, L. He, D. D. Wei and Q. B. Yuan, *J. Am. Ceram. Soc.*, 2015, **98**, 528. View Article Online
DOI: 10.1039/C7TC01718A
- 18 G. Q. Zhang, J. Guo, L. He, D. Zhou, H. Wang, J. Koruza and M. Kosec, *J. Am. Ceram. Soc.*, 2014, **97**, 241.
- 19 H. Kähäri, M. Teirikangas, J. Juuti and H. Jantunen, *J. Am. Ceram. Soc.*, 2014, **97**, 3378.
- 20 H. Kähäri, M. Teirikangas, J. Juuti and H. Jantunen, *J. Am. Ceram. Soc.*, 2015, **98**, 687.
- 21 H. Kähäri, M. Teirikangas, J. Juuti and H. Jantunen, *Ceram. Int.*, 2016, **42**, 11442.
- 22 J. Guo, S. S. Berbano, H. Guo, A. L. Baker, M. T. Lanagan and C. A. Randall, *Adv. Funct. Mater.*, 2016, **26**, 7115.
- 23 D. Zhou, W. B. Li, L. X. Pang, J. Guo, Z. M. Qi, T. Shao, Z. X. Yue and X. Yao, *J. Am. Ceram. Soc.*, 2014, **97**, 3597.
- 24 M. Gracia, J. F. Marco, J. R. Gancedo, J. L. Gautier, E. I. Ríos, N. Menéndez and J. Tornero, *J. Mater. Chem.*, 2003, **13**, 844.
- 25 D. S. Mathew and R. S. Juang, *Chem. Eng. J.*, 2007, **129**, 51.
- 26 V. G. Harris, A. Geiler, Y. Chen, S. D. Yoon, M. Wu, A. Yang, Z. Chen, P. He, P. V. Parimi, X. Zuo, C. E. Patton, M. Abe, O. Acher and C. Vittoria, *J. Magn. Magn. Mater.*, 2009, **321**, 2035.
- 27 W. C. Tsai, Y. H. Liou, Y. C. Liou, *Mater. Sci. Eng. B*, 2012, **177**, 1133.
- 28 A. Feteira, *J. Am. Ceram. Soc.*, 2009, **92**, 967.
- 29 J. Donohue and W. Shand, *J. Am. Chem. Soc.*, 1947, **69**, 222.
- 30 K. G. Bramnik and H. Ehrenberg, *Z. Anorg. Allg. Chem.*, 2004, **630**, 1336.
- 31 D. R. Lide, *CRC Handbook of Chemistry and Physics (90th ed.)*. Boca Raton, Florida: CRC Press (2009).

- 32 J. A. Dean, *Lange's Handbook of Chemistry 16th Edition*, McGraw-Hill, INC. (1999). View Article Online
DOI: 10.1039/C7TC01718A
- 33 A. Bouhemadou, R. Khenata, D. Rached, F. Zerarga and M. Maamache, *Eur. Phys. J. Appl. Phys.*, 2007, **38**, 203.
- 34 K. Momma and F. Izumi, *J. Appl. Crystallogr.*, 2011, **44**, 1272.
- 35 R. D. Shannon, *Acta Crystallogr. Sect. A: Cryst. Phys. Diffr. Theor. Gen. Crystallogr.*, 1976, **32**, 751.
- 36 D. Zhou, H. Wang, X. Yao and L. X. Pang, *J. Am. Ceram. Soc.*, 2008, **91**, 2228.
- 37 D. Zhou, L. X. Pang, Z. M. Qi and X. Yao, *Inor. Chem.*, 2014, **53**, 9222.
- 38 G. P. Donati, R. Kaspi and K. J. Malloy, *J. Appl. Phys.*, 2003, **94**, 5814.
- 39 S. Adachi, *Properties of Semiconductor Alloys: Group-IV, III–V and II–VI Semiconductors*, Wiley, New York (2009).
- 40 J. V. B. Moura, J. G. da Silva Filho, P. T. C. Freire, C. Luz-Lima, G. S. Pinheiro, B. C. Viana, J. Mendes Filho, A. G. Souza-Filho and G. D. Saraiva, *Vib. Spectrosc.*, 2016, **86**, 97.
- 41 G. D. Saraiva, W. Paraguassu, M. Maczka, P. T. C. Freire, Jr. J. A. Lima, C. W. A. Paschoal, J. Mendes Filho and A. G. Souza Filho, *J. Raman Spectrosc.*, 2008, **39**, 937.
- 42 V.P. Mahadevan Pillai, T. Pradeep, M. J. Bushiri, R. S. Jayasree and V.U. Nayar, *Spectrochimica Acta Part A*, 1997, **53**, 867.
- 43 R. H. Busey and Jr. O. L. J. *Chem. Phys.*, 1964, **41**, 215.
- 44 F. D. Hardcastle and I. E. Wachs, *J. Raman Spectrosc.*, 1990, **21**, 683.
- 45 D. Zhou, L. X. Pang, H. D. Xie, J. Guo, B. He, Z. M. Qi, T. Shao, X. Yao and C. A. Randall, *Eur. J. Inorg. Chem.*, 2014, **2**, 296.
- 46 G. K. Choi, J. R. Kim, S. H. Yoon and K. S. Hong, *J. Eur. Ceram. Soc.*, 2007, **27**, 3063.

47 R. D. Shannon, *J. Appl. Phys.*, 1993, **73**, 348.

[View Article Online](#)
DOI: 10.1039/C7TC01718A

48 I. S. Cho, D. W. Kim, J. R. Kim and K. S. Hong, *Ceram. Int.*, 2004, **30**, 1181.

Table 1 Refined atomic fractional coordinates from XRD data for the (Na_{1.2}Ag_{0.8})MoO₄ sample and the lattice parameters at room temperature are $a = b = c$

$= 9.202\ (0)\ \text{\AA}$. The space group is Fd-3m (227).

Atom	Site	Occ.	x	y	z	Biso
Mo	8a	0.04167	0.12500	0.12500	0.12500	0.67564
Na	16d	0.05000	0.50000	0.50000	0.50000	1.15366
Ag	16d	0.03333	0.50000	0.50000	0.50000	1.15366
O	32e	0.16667	0.23460	0.23460	0.23460	0.76760

Table 2 Refined atomic fractional coordinates from XRD data for the

View Article Online
DOI: 10.1039/C7TC01718A

(Na_{1.8}Ag_{0.2})MoO₄ sample and the lattice parameters at room temperature are $a = b = c = 9.133 (5) \text{ \AA}$. The space group is Fd-3m (227).

Atom	Site	Occ.	x	y	z	Biso
Mo	8a	0.04167	0.12500	0.12500	0.12500	0.32704
Na	16d	0.07500	0.50000	0.50000	0.50000	0.78023
Ag	16d	0.00833	0.50000	0.50000	0.50000	0.78023
O	32e	0.16667	0.23460	0.23460	0.23460	0.59198

Table 3 Comparison of microwave dielectric properties of ULTCCs with a permittivity ~ 8

View Article Online
DOI: 10.1039/C7TC01718A

Composition	Phase	S.T. (°C)	ϵ_r	Qf (GHz)	TCF (ppm/°C)	Ref.
NaAgMoO ₄	spinel	400	7.9	33,000	−120	14
Li ₂ O-B ₂ O ₃ -SiO ₂ -Al ₂ O ₃ -CaO	composite	550	8.0	2,400	−48	48
Ag ₂ MoO ₄	spinel	450	8.1	17,000	−133	23
(Na _{1.2} Ag _{0.8})MoO ₄	spinel	410	8.1	44,800	−82	this work
Li ₂ Ca ₂ Mo ₃ O ₁₂	composite	630	8.5	108,000	−89	5
Li ₂ Mo ₄ O ₁₃	Anorthic	520	8.8	7,700	−66	16

Figure Captions

View Article Online
DOI: 10.1039/C7TC01718A

Fig. 1 X-ray diffraction patterns of the $(\text{Na}_x\text{Ag}_{2-x})\text{MoO}_4$ ($0 \leq x \leq 2$) ceramics sintered at optimal temperatures (a), the experimental (circles) and calculated (line) X-ray powder diffraction profiles of the $(\text{Na}_{1.2}\text{Ag}_{0.8})\text{MoO}_4$ ceramic sintered at 410 °C for 2 h ($R_p = 11.9\%$, $R_{wp} = 14.3\%$, $R_{exp} = 7.07\%$) (b), the $(\text{Na}_{1.8}\text{Ag}_{0.2})\text{MoO}_4$ ceramic sintered at 470 °C (c) for 2 h ($R_p = 8.32\%$, $R_{wp} = 10.5\%$, $R_{exp} = 5.91\%$, the short vertical lines below the patterns mark the positions of Bragg reflections. The bottom continuous line is the difference between the observed and the calculated intensity), XRD patterns of the $(\text{Na}_{1.2}\text{Ag}_{0.8})\text{MoO}_4$ co-fired samples with 30 wt. % Ag and 30 wt. % Al at 410 °C for 2 h (d), and schematic crystal structure of the $(\text{Na}_x\text{Ag}_{2-x})\text{MoO}_4$ ceramic (e).

Fig. 2 SEM images of as-fired and fractured surfaces of the $(\text{Na}_{1.2}\text{Ag}_{0.8})\text{MoO}_4$ ceramic sintered 410 °C (a) and densification temperatures of the $(\text{Na}_x\text{Ag}_{2-x})\text{MoO}_4$ ceramics as a function of x with relative density marked (b).

Fig. 3 Raman spectra of the $(\text{Na}_x\text{Ag}_{2-x})\text{MoO}_4$ ($0 \leq x \leq 2$) ceramics (a) and mode shift as a function of x (b).

Fig. 4 Microwave dielectric permittivity, Qf value and TCF value of the $(\text{Na}_x\text{Ag}_{2-x})\text{MoO}_4$ ($0 \leq x \leq 2$) ceramics as a function of x.

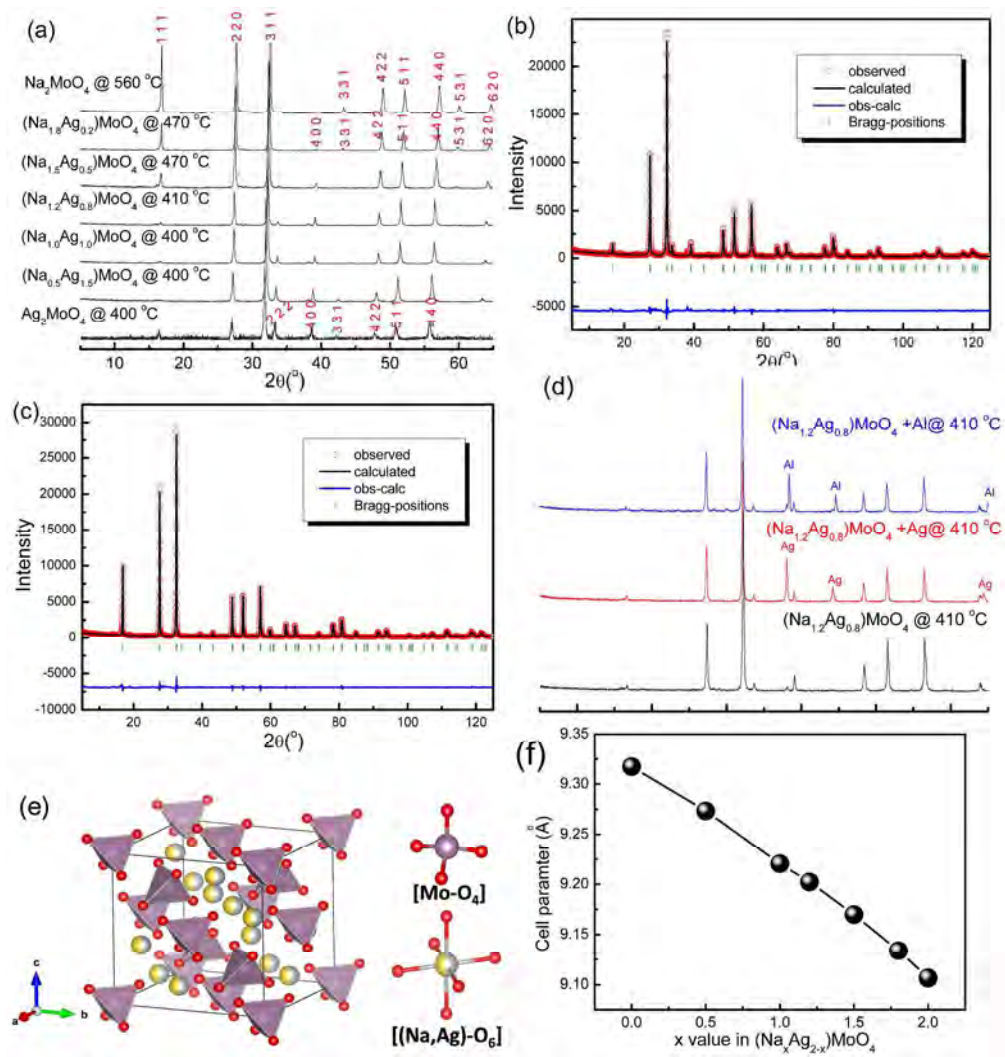


Fig. 1 X-ray diffraction patterns of the $(\text{Na}_x\text{Ag}_{2-x})\text{MoO}_4$ ($0 \leq x \leq 2$) ceramics sintered at optimal temperatures (a), the experimental (circles) and calculated (line) X-ray powder diffraction profiles of the $(\text{Na}_{1.2}\text{Ag}_{0.8})\text{MoO}_4$ ceramic sintered at 410 °C for 2 h ($R_p = 11.9\%$, $R_{wp} = 14.3\%$, $R_{exp} = 7.07\%$) (b), the $(\text{Na}_{1.8}\text{Ag}_{0.2})\text{MoO}_4$ ceramic sintered at 470 °C (c) for 2 h ($R_p = 8.32\%$, $R_{wp} = 10.5\%$, $R_{exp} = 5.91\%$, the short vertical lines below the patterns mark the positions of Bragg reflections. The bottom continuous line is the difference between the observed and the calculated intensity), XRD patterns of the $(\text{Na}_{1.2}\text{Ag}_{0.8})\text{MoO}_4$ co-fired samples with 30 wt. % Ag and 30 wt. % Al at 410 °C for 2 h (d), and schematic crystal structure of the $(\text{Na}_x\text{Ag}_{2-x})\text{MoO}_4$ ceramic (e).

268x281mm (300 x 300 DPI)

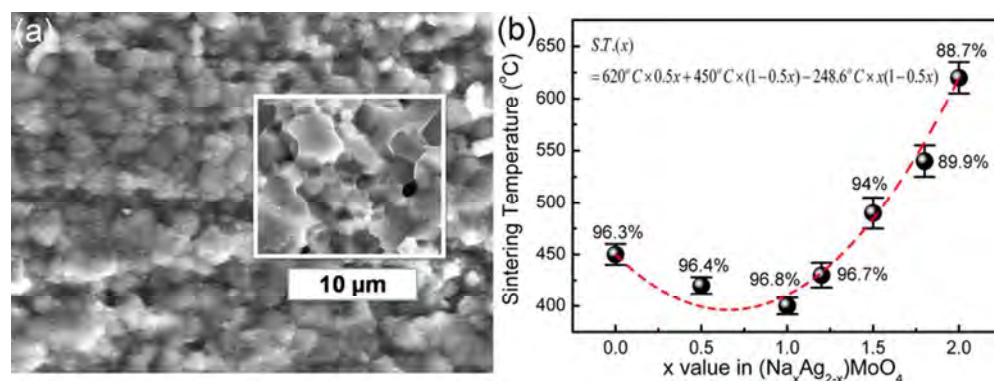


Fig. 2 SEM images of as-fired and fractured surfaces of the $(\text{Na}_{1.2}\text{Ag}_{0.8})\text{MoO}_4$ ceramic sintered 410 °C (a) and densification temperatures of the $(\text{Na}_x\text{Ag}_{2-x})\text{MoO}_4$ ceramics as a function of x with relative density marked (b).

74x28mm (300 x 300 DPI)

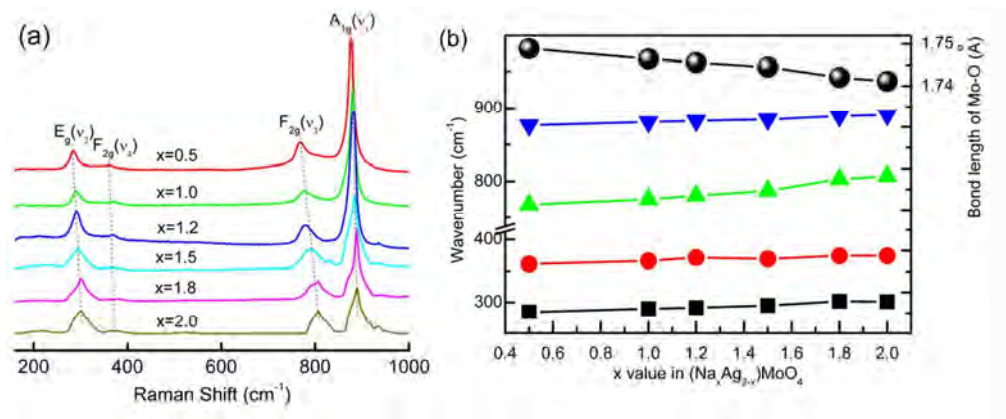


Fig. 3 Raman spectra of the $(\text{Na}_x\text{Ag}_{2-x})\text{MoO}_4$ ($0 \leq x \leq 2$) ceramics (a) and mode shift as a function of x (b).

90x37mm (300 x 300 DPI)

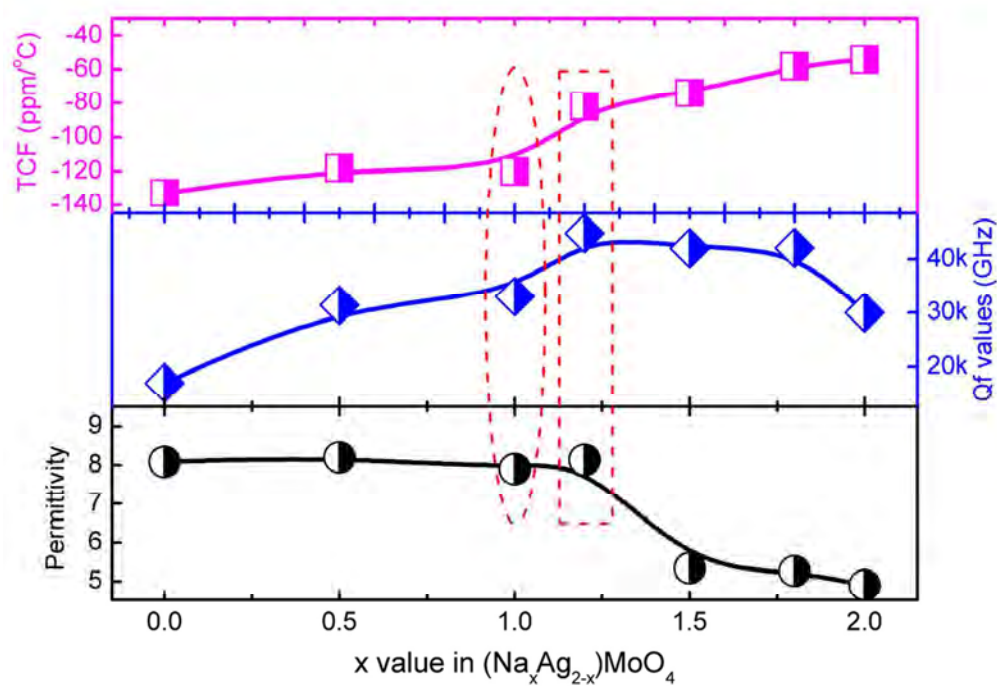


Fig. 4 Microwave dielectric permittivity, Qf value and TCF value of the $(\text{Na}_x\text{Ag}_{2-x})\text{MoO}_4$ ($0 \leq x \leq 2$) ceramics as a function of x.

88x62mm (300 x 300 DPI)

TOC GRAPH:

TOC Synopsis: A novel series of spinel structured ultra-low temperature co-fired microwave dielectric $(\text{Na},\text{Ag})\text{MoO}_4$ ceramics were studied in detail. The $(\text{Na}_{1.2}\text{Ag}_{0.8})\text{MoO}_4$ ceramic can be well sintered at 410°C with a permittivity ~ 8.1 , a quality factor (Q_f) $\sim 44,800\text{ GHz}$ and grain size $1 \sim 5\text{ }\mu\text{m}$.

